



Measurement of the para-hydrogen concentration in the ISIS moderators using neutron transmission and thermal conductivity



Giovanni Romanelli ^{a,b,*}, Svemir Rudić ^a, Matteo Zanetti ^{a,c}, Carla Andreani ^{b,e},
Felix Fernandez-Alonso ^{a,f}, Giuseppe Gorini ^c, Maciej Krzystyniak ^{a,d}, Goran Škoro ^a

^a ISIS Facility, Rutherford Appleton Laboratory, Chilton, Didcot, Oxfordshire OX11 0QX, UK

^b Università degli Studi di Roma 'Tor Vergata', Dipartimento di Fisica and NAST Centre, Via della Ricerca Scientifica 1, 00133, Roma, Italy

^c Università di Milano Bicocca, Piazza della Scienza 3, Milano 20125, Italy

^d School of Science and Technology, Nottingham Trent University, Clifton Campus, Nottingham, NG11 8NS, UK

^e Museo Storico della Fisica e Centro Studi e Ricerche Enrico Fermi, Piazza del Viminale 1, Italy

^f Department of Physics and Astronomy, University College London, Gower Street, London, WC1E 6BT, UK

ARTICLE INFO

Keywords:

Neutron transmission
Neutron cross sections
Hydrogen thermal conductivity
Para hydrogen
Neutron moderators

ABSTRACT

We present an experimental study to determine the para-hydrogen concentration in the hydrogen moderators at the ISIS pulsed neutron and muon source. The experimental characterisation is based on neutron transmission experiments performed on the VESUVIO spectrometer, and thermal conductivity measurements using the TOSCA para-hydrogen rig. A reliable estimation of the level of para-hydrogen concentration in the hydrogen moderators is of crucial importance in the framework of a current project to completely refurbish the first target station at ISIS. Moreover, we report a new measurement of the total neutron cross section for normal hydrogen at 15 K on the broad energy range 3 meV–10 eV suggesting a revision of the most recent nuclear libraries for incident neutron energies lower than 10 meV. Finally, we characterise systematic errors affecting the para-hydrogen level estimation due to conversion from para to ortho hydrogen, as a function of the time a batch of gas spends in every component of our gas panel and apparatus.

© 2018 Elsevier B.V. All rights reserved.

1. Introduction

The ISIS pulsed neutron and muon source [1] is a leading centre for neutron science. The facility offers a growing suite of instruments employing neutrons produced by two target stations. While the second target station (TS2) is relatively new, having been inaugurated in 2008, the first target station (TS1) produced the first neutron in 1984, and is now the subject of a complete refurbishment, including the design of the target and its cooling systems, the moderators, the reflector, and all their associated services. In the framework of this project, attention needs to be paid on a careful characterisation of the baseline representing the actual state of the TS1 components, so as to obtain optimal gains. Both target stations have coupled hydrogen moderators, that will be the focus of this work.

Molecular hydrogen (H₂) in the liquid phase is a typical moderating material, enabling intense fluxes of cold neutrons. The molecule can be found in two nuclear-spin configurations: when hydrogen (H) nuclei have parallel spins, the molecule is referred to as ortho hydrogen (oH)

with total nuclear spin $I = 1$ and degeneracy $2I + 1 = 3$; conversely, the singlet state obtained when the two spins are anti-parallel is referred to as para hydrogen (pH).

The effect of quantum mechanics on the two spin isomers is dramatic. The nuclear spin wave function has a symmetry $(-1)^{I+1}$, therefore being antisymmetric for pH and symmetric for oH. In order to have an overall antisymmetric nuclear wave function, as a consequence of the Fermi–Dirac statistics for protons, the nuclear rotational densities of states of pH and oH can only include energy levels corresponding to even and odd rotational quantum numbers J , respectively. As the energy of pH ground state is ca. 14.5 meV lower than in oH, the latter is slowly converted to the former when a gas mixture is cooled to low temperatures. The conversion rate can be of the order of weeks, and paramagnetic catalysts are often used to speed it up to time scale of days [2,3].

The difference between oH and pH thermal conductivities is an interesting example of the reflection of quantum mechanics into a macroscopic physical quantity. Of an even greater interest is the difference between the neutron cross sections in the two cases [6,7] shown in

* Corresponding author at: ISIS Facility, Rutherford Appleton Laboratory, Chilton, Didcot, Oxfordshire OX11 0QX, UK.
E-mail address: giovanni.romanelli@stfc.ac.uk (G. Romanelli).

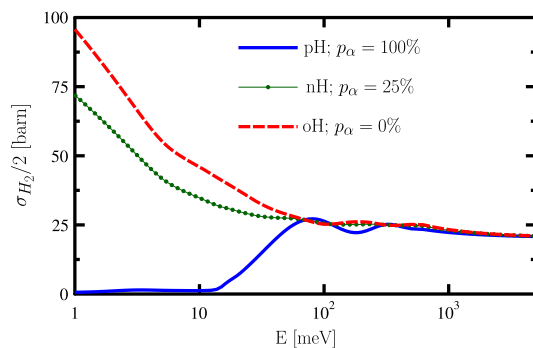


Fig. 1. Neutron cross sections for pH, oH, and normal hydrogen (nH) taken from the ENDF/B-VII library [4,5]. The three curves correspond to a pH concentration $p_\alpha = 100\%$ (blue solid line), 25% (green dotted line), and 0% (red dashed line), respectively.

Fig. 1. In the case of pH, the proximity of the two Hs in the molecule and their opposite spins leads to destructive interference between scattered neutron waves with a wavelength large enough to match the size of the entire molecule. Therefore, the neutron cross section is largely suppressed for cold neutrons, while it has the same epithermal limit as oH, *i.e.*, the free H cross section at ca. 20.5 b [8,9].

The problem of the determination of the pH concentration in neutron moderators has been tackled with several techniques in the last decades. Recent approaches [10,11] are based on Raman spectroscopy and aim for *in situ* and real-time assessments of the pH concentration in liquid hydrogen moderators. Yet, experiments can be only performed on the flow stream into a small gas chamber, possibly several metres away from the liquid moderator. For example, Ref. [10] reports an accuracy of 4% in the pH estimation by analysing the relative intensities of the first-order Raman lines for oH and pH. Similarly, neutron vibrational spectroscopy has been used to monitor the conversion rate of pH to oH in the presence of catalysts [12]. Neutron Transmission (NT) is a technique capable of probing a representative sample directly extracted from a liquid-hydrogen moderator, and assess the percentage of pH by exploiting the aforementioned difference of pH and oH cross sections. However, the determination of these cross sections has proven a challenging task. Pioneering experiments by Seiffert [13], later complemented by additional experiments [14] and modelling [15–17] provided the input for the ENDF/B-VII nuclear libraries [4,5], generally used in neutron transport simulations. However, recent research [7,18] has suggested that the original experimental data underestimated the percentage of oH in the pH sample, therefore overestimating the pH cross section below ca. 10 meV.

In the following sections, we present an experimental procedure to establish the concentration of pH in the ISIS moderators. In particular, Section 2 discusses the collection and preparation of the H_2 samples, together with the theory behind NT and thermal conductivity (TC) measurements. Moreover, we report in Section 3 the results of our experiments including: (i) NT experiments to characterise two reference gas mixtures; (ii) the calibration procedure to convert TC measurements into estimates of the pH concentration in a gas mixture, hereafter referred to as p_α ; (iii) additional tests using NT to confirm such calibration procedure; and (iv) systematic conversion of pH into oH as the gas is stored in each element of our apparatus. Finally, conclusions are drawn in Section 4.

2. Materials and methods

A schematic diagram of the experimental apparatus [19] is shown in Fig. 2, and it is discussed in detail in this section.

2.1. Sample preparation

Pure H_2 was obtained as a commercially available sample from CK Gas [20]. After its storage in a stainless steel (SS) container at room temperature for a period in excess of few weeks, it was considered to have been equilibrated to the state of normal hydrogen (nH). We define nH as the classical limit of a thermodynamic equilibrium mixture of oH and pH. When the gas is stored at room temperature, away from the quantum regime, differences between oH and pH energy levels are negligible with respect to $k_B T$, and the ratio of concentrations of the two states is 3:1, *i.e.*, the ratio of triplet-to-singlet nuclear-spin degeneracies. Therefore, we can assume $p_\alpha = 25\%$ in the case of nH.

Samples from the ISIS hydrogen moderators were collected at the end of the experimental cycle of operations in October 2016, and stored in PTFE-coated SS bottles and kept at room temperature. The decision on the type of bottles where to store a gas mixture was made so as to minimise pH converting to oH. A discussion on other possible materials for the storage bottles is presented in Section 3.5.

Finally, the preparation of a mixture with a high p_α was possible owing to the TOSCA pH rig [21,22], hereafter referred to as the rig. We shall denote the pH concentration in this case p_r . The rig was built at ISIS for use on the TOSCA spectrometer, so as to prepare gas mixtures with p_α as high as possible, and measure p_α in a gas mixture prior or after absorption in materials. This characterisation is possible owing to thermal conductivity measurements, discussed below. The rig is composed of a 10 K cold head assembly, a pumping set, a gas handling system, an aluminium cell where pH is generated and stored, hereafter referred to as the generation cell, and a temperature control system. The generation cell has a cylindrical geometry with a radius of 4.5 cm and height of 10.5 cm, and contains ca. 50 g of CrO_3 powder from Oxisorb[®] Oxygen Scrubber [23] acting as a catalyst to convert oH into pH [12].

2.2. Neutron transmission experiments

Neutron transmission experiments were performed on the VESUVIO instrument [24,25] at ISIS. VESUVIO is an inverted-geometry spectrometer mainly employed for the determination of nuclear quantum effects in materials using Deep Inelastic Neutron Scattering [26]. In recent years, VESUVIO has become an epithermal and thermal analysis station [25], where samples can be investigated through spectroscopy [27,28], neutron diffraction [29,30], and NT [31] at the same time. The energy range accessible for NT spans 8 orders of magnitude, from a fraction of meV to tens of keV.

Samples were placed at ca. 11 m from the TS1 water moderator. Incident neutron spectra were recorded using a GS20 ⁶Li-doped scintillator at ca. 8.57 m from the moderator, while the transmitted spectra were recorded using a similar detector at a distance 13.45 m from the moderator. The neutron beam has a circular shape, with a maximum diameter of ca. 4.5 cm. Due to the small solid angle seen by the transmitted monitor, we assume the counts due to scattering in the sample to be negligible. Moreover, the shape of the neutron beam at the sample position does not depend upon incident energy [25]. Therefore, divergence of the beam between the sample position and the position of the transmitted monitor can be neglected. The Beer–Lambert law for the transmission $T_\alpha(E)$, as a function of the incident neutron energy E , reads

$$T_\alpha(E) = \frac{S_\alpha(E) - B(E)}{C(E) - B(E)} \simeq \frac{S_\alpha(E)}{C(E)} = \exp(-n\sigma_\alpha(E)d), \quad (1)$$

where $S_\alpha(E)$ is the spectrum from the sample α in the container, $C(E)$ is the corresponding spectrum for empty container, $B(E)$ is a sample-independent background, n is the sample number density, and d is the thickness of the sample volume in the direction of the incident beam. Moreover, $\sigma_\alpha(E)$ is the energy-dependent neutron cross section of the gas mixture, expressed as a linear combination of the pH and oH cross sections, $\sigma_p(E)$ and $\sigma_o(E)$ respectively

$$\sigma_\alpha(E) = p_\alpha \sigma_p(E) + (1 - p_\alpha) \sigma_o(E). \quad (2)$$

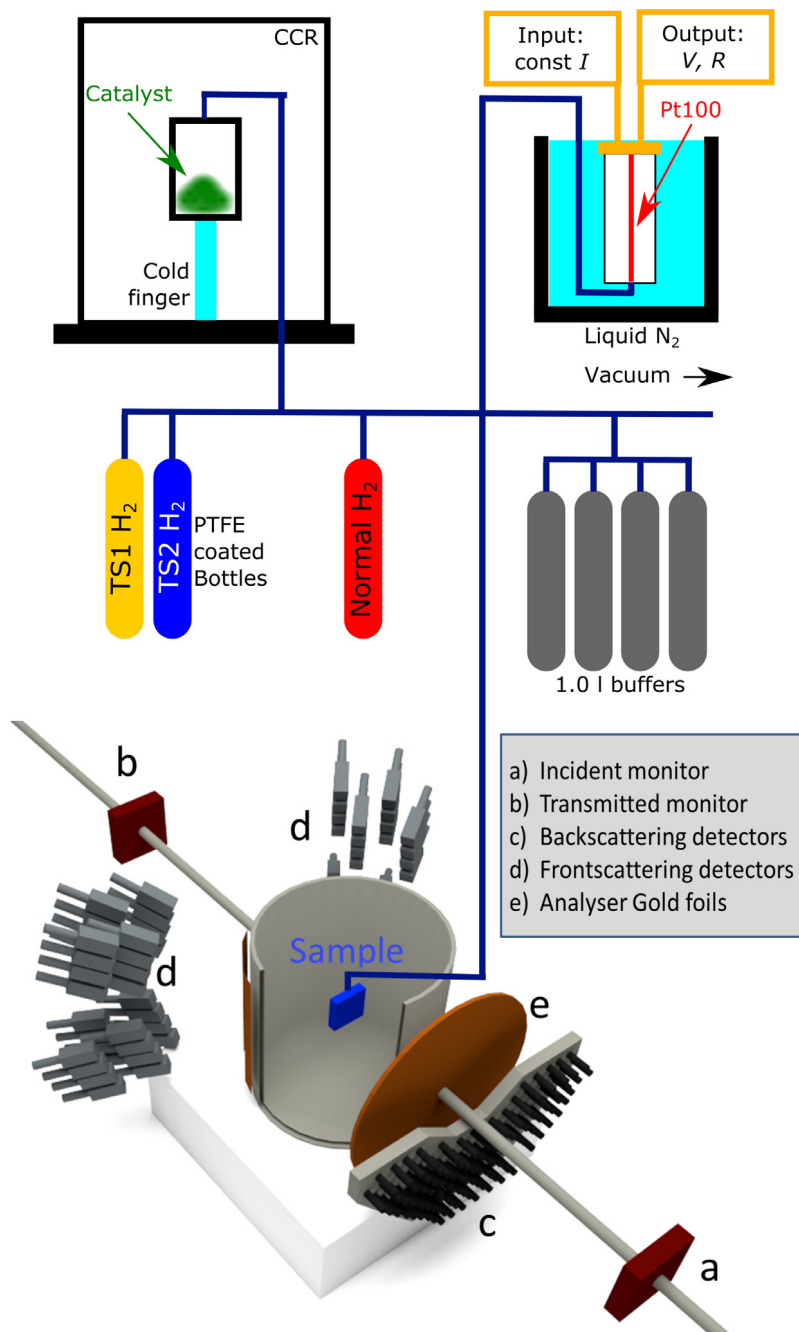


Fig. 2. Schematic diagram of the experimental set up including: pH generation cell containing the catalyst powder and inserted in a cold-finger closed-circuit refrigerator (top left); the gauge cell for TC measurements inserted in a liquid-nitrogen bath, and equipped with a Pt100 sensor attached constant-current source (top right); PTFE-coated bottles containing H_2 from the liquid-hydrogen ISIS moderators, commercially available nH, and SS buffers (middle); and the VESUVIO spectrometer (bottom).

Two containers were used in the NT measurements. Container #1 was a flat square aluminium can with sample thickness $d_1 = 0.5$ mm, area $6.4 \text{ cm} \times 6.4 \text{ cm}$, and thickness of each wall equal to 5 mm. Container #2 was a flat circular aluminium can with sample thickness $d_2 = 1$ mm, diameter 5 cm, and thickness of each wall equal to 1 mm. Container #2 was optimal for the NT measurements on VESUVIO, yet it was not available for the measurement on nH, and container #1 had to be used instead. Measurements were performed at 15 K, where H_2 is a liquid with mass density 0.076 g/cm^3 . To achieve the desired temperature, the standard VESUVIO closed-circuit refrigerator was used. The background $B(E)$ has been measured several times on the VESUVIO spectrometer placing a 1-mm-thick Cadmium foil at the beginning of the VESUVIO blockhouse, ca. 2 m before the sample along the beam line, and it was found to be negligible.

2.3. Thermal conductivity measurements

The rig is equipped with a cylindrical aluminium container, here referred to as the *gauge cell*, used to perform thermal conductivity measurements. The working principle is that a heat source suspended in a medium dissipates energy at a rate proportional to the thermal conductivity of the medium and the thermal gradient. In our set-up, the heat source is a platinum wire at the centre of the cylinder, where power is generated as a current flows in it. As shown in Fig. 3, the thermal conductivity of pH and nH can be as different as 20% at ca. 150 K and ca. 1 bar [32]. The temperature dependence of the thermal conductivities of pH, oH, and nH is reported in Fig. 3. An empirical definition of H_2 thermal conductivity was given in Ref. [32] and

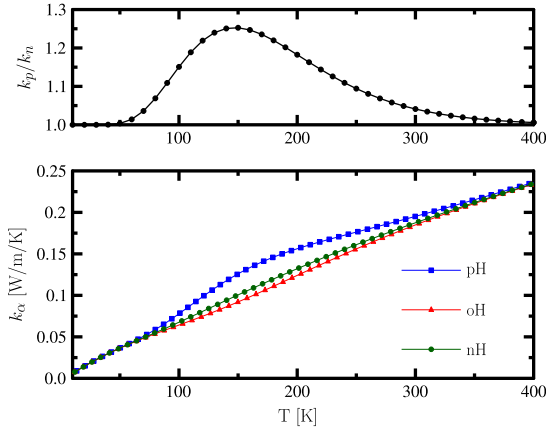


Fig. 3. Thermal conductivity of nH (green circles), pH (blue squares), and oH (red triangles) in the gas phase (bottom panel), and the ratio of para-to-normal thermal conductivities (top panel). Results obtained using the models described in Ref. [32] at ca. 1 bar.

reads

$$k_{\alpha}(T) = [a_0 + a_1 T + (b_0 + b_1 T) C_{\alpha}(T)] \frac{\eta(T)}{M(1 + c/T)}, \quad (3)$$

where the parameters $a_0 = 1.8341$, $a_1 = -0.0045$, $b_0 = 1.1308$, $b_1 = 0.0009$, and $c = 3.2$ had been fitted to reproduce experimental data at a pressure of 1 bar. Moreover, M is the mass of H_2 in atomic mass units, C_{α} is the specific heat at constant pressure expressed in calories per Kelvin per mole. An analytical definition of the heat capacity $C_{v,\alpha}$ at constant volume can be obtained from the vibrational density of states for molecular oH and pH in the rigid rotor approximation. We then assumed $C_{\alpha} = C_{v,\alpha} + \mathcal{R}$, where \mathcal{R} is the ideal gas constant. Also, $\eta(T)$ being the viscosity of H_2 , was considered to be the same for oH and pH, and it was expressed in the same Ref. [32] in poises, and T in K, as

$$\eta(T) = 85.558 \times 10^{-7} \frac{T^{3/2}}{T + 19.95} \frac{T + 650.39}{T + 1175.9}. \quad (4)$$

The validity of the Mayer's Formula relating heat capacities and the assumption that pH and oH have the same viscosity were checked against Tables 2 and 8 of Ref. [33]. The empirical definition of the thermal conductivity of H_2 gas in Eq. (3) was compared with a simpler and generally accepted Eucken's equation [34]

$$k_{\alpha}(T) = \left(C_{\alpha}(T) + \frac{9}{4} \mathcal{R} \right) \frac{\eta(T)}{M}, \quad (5)$$

and was found to give reliable results.

The equation of thermal conduction for a steady-state gas in a volume with axial symmetry reads $d\dot{Q}/dr = 0$, where \dot{Q} is the heat flow rate through a cylindrical surface $2\pi r l$ at a distance r from the axis and with height l . The gas experiences a temperature gradient along the radial direction, dT/dr , between the hot temperature of the wire, T_{α} , and the cold temperature of the walls of the container, $T_0 = 77$ K, immersed in the liquid nitrogen bath. When the equation of thermal conduction is integrated between the radius of the wire, r_0 , and the radius of the cylinder, r , one has

$$\frac{1}{R(T_{\alpha})} \int_{T_0}^{T_{\alpha}} k_{\alpha}(T) dT = \frac{I^2 \ln(r/r_0)}{2\pi l} = A, \quad (6)$$

where the heat flow rate $\dot{Q} = R(T)I^2$ has been replaced by the product of the constant current $I = 100$ mA flowing in the wire, and the temperature-dependent resistance $R(T)$. On the left-hand side of Eq. (6) one has a term related to the thermodynamic properties of the gas and dependent on the temperature of the wire T_{α} . The term in the centre of Eq. (6) is related to the geometry of the container and to the constant value of the current in the wire, and it remains unchanged for different gases. Therefore, we consider this term a constant parameter A , defined

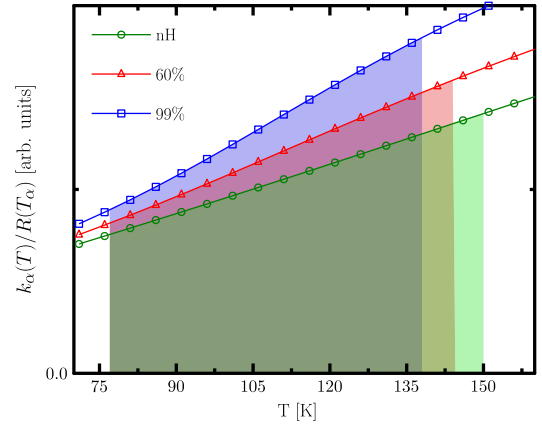


Fig. 4. Thermal conductivity $k_{\alpha}(T)$ divided by the resistance of the wire $R(T_{\alpha})$ for H_2 in the gas phase, and in the case of nH (green circles), $p_{\alpha} = 60\%$ (red triangles), and $p_{\alpha} = 99\%$ (blue squares).

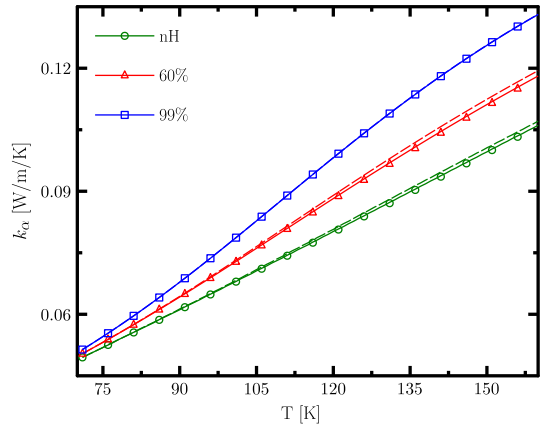


Fig. 5. Thermal conductivity of an H_2 gas in the case of nH (green circles), $p_{\alpha} = 60\%$ (red triangles), and $p_{\alpha} = 99\%$ (blue squares). In particular, solid lines correspond to Eq. (7), markers correspond to Eq. (8), and dashed lines (often almost overlapping to the solid lines) correspond to Eq. (10).

in the right-hand side of the equation. One should note that Eq. (6) holds in the case of negligible convection modes only, and in reality one can expect slight deviations in the value of A depending on the temperature of the wire. The temperature T_{α} was obtained from the measured resistance of the wire through the calibration line $R(T) = 100 + 0.4064(T - 273)$, with the temperature expressed in K and the resistance in Ω . The calibration was based on the resistance when a negligible current $I = 1$ mA was flowing in the wire, and when the gauge cell was at thermal equilibrium at room temperature and at liquid-nitrogen temperature. Calibration curves of Pt100 sensors can be found in Ref. [35], and are compatible with our calibration.

Fig. 4 pictorially exemplifies the meaning of Eq. (6). The integral corresponds to the area subtended by the curve $k_{\alpha}(T)$ in the range between liquid nitrogen temperature and the temperature of the wire. Gas mixtures with higher thermal conductivity allow for lower temperatures of the wire. The simultaneous change of the intensity of the thermal conductivity and the upper limit of integration, make the absolute value of the integral a constant.

The thermal conductivity of a mixture of gases can be approximated in several ways. Ref. [36] suggests a definition of the form

$$k_{\alpha} = k_p^{p_{\alpha}} k_o^{1-p_{\alpha}}, \quad (7)$$

and the resulting thermal conductivity as a function of temperature for three gas mixtures is reported in Fig. 5 as a solid line. Elsewhere [37],

the thermal conductivity is expressed as

$$k_\alpha = \frac{k_p}{1 + G_{p\alpha} \frac{1-p_\alpha}{p_\alpha}} + \frac{k_o}{1 + G_{o\alpha} \frac{p_\alpha}{1-p_\alpha}}, \quad (8)$$

with the coefficients

$$G_{ij} = \frac{1}{\sqrt{8}} \left(1 + \frac{M_i}{M_j}\right)^{-\frac{1}{2}} \left[1 + \sqrt{\frac{M_i k_i}{M_j k_j}}\right]^2 = \frac{1}{4} \left[1 + \sqrt{\frac{k_i}{k_j}}\right]^2. \quad (9)$$

The last equality holds for gases with the same molar mass $M_i = M_j$, as in our case. The resulting thermal conductivity is reported in Fig. 5 as markers. The coefficients G_{ij} are approximately one, in which limit the thermal conductivity can be expressed in a much simpler way,

$$k_\alpha(T) = p_\alpha k_p(T) + (1 - p_\alpha) k_o(T). \quad (10)$$

Fig. 5 shows the latter case as well, as dashed lines. Comparisons of the three models are presented in the case of nH and gas mixtures with $p_\alpha = 60\%$ and $p_\alpha = 99\%$. The models from Eq. (7) and from Eq. (8) perfectly overlap over the entire temperature range considered here. On the other hand, Eq. (10) slightly overestimates the thermal conductivity with respect to the other two models. However, differences between the three models when Eq. (6) is applied are much smaller than other sources of errors in the experimental procedure described in this work, and Eq. (10) is chosen for the sake of simplicity.

Consequently, one can express the pH concentration in an unknown gas mixture as a function of known values in the case of nH and the temperature of the wire, as

$$p_\alpha = \frac{\frac{R(T_\alpha)}{R(T_n)} \int_{T_0}^{T_n} k_n(T) dT - \int_{T_0}^{T_\alpha} k_o(T) dT}{\int_{T_0}^{T_\alpha} [k_p(T) - k_o(T)] dT}, \quad (11)$$

where T_n and T_α are the temperatures of the wire when nH and a gas mixture α are inserted in the gauge cell, respectively.

3. Results

Ideally, Eq. (11) only requires one reference sample in order to obtain p_α for an unknown mixture, say nH. However, we will base the following discussion on the use of two reference points in order to remove any dependence on our assumptions, such as negligible convection modes. To do this, a second reference point needs to be characterised, and we chose as the second sample the gas generated within the rig.

3.1. Concentration of pH obtained in the rig

The percentage of pH in the mixture generated within the rig is, in principle, unknown. The generation process is based on the condensation of nH inside the conversion cell, where a catalyst is placed. The low temperature of ca. 10 K, and the action of the catalyst are expected to boost the conversion from oH to pH within few days. During this period, solid H_2 is slightly warmed for a short time, so as to go back to the gas phase and condensate again around the catalyst. This is done to allow as many molecules as possible to interact with the catalyst.

In order to assess the pH concentration in the gas generated within the rig, NT experiments were performed. To test the quality of our results, the first experiment was performed on a nH mixture loaded in the sample container #1 at 15 K. The duration of the measurement was ca. 8 h, and separate spectra were recorded every ca. 30 min. No conversion was observed during this period, and we estimate a negligible conversion during the loading process when the gas goes directly from the generation cell to the VESUVIO cell, as discussed later in Section 3.5. The resulting cross section, expressed in barn per atom, is shown in Fig. 6 as green circles, and it is compared with the tabulated values in the ENDF/B-VII for oH and pH combined using $p_\alpha = 25\%$. As the tabulated values corresponded to the scattering cross section only,

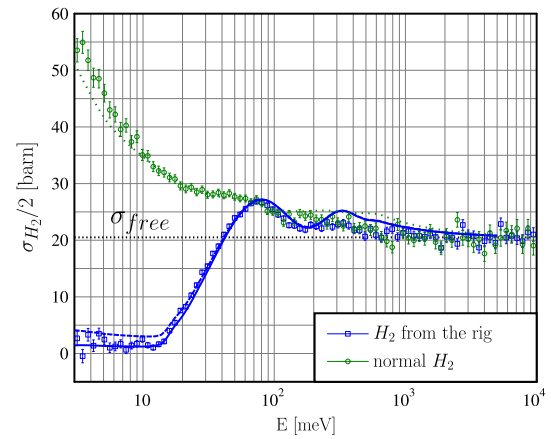


Fig. 6. Neutron cross section per H atom for nH (green circles) and a sample obtained from the rig (blue squares). Lines correspond to linear combination of oH and pH scattering cross sections obtained from the ENDF/B-VII library, in the cases $p_\alpha = 25\%$ (green dotted line), $p_\alpha = 96\%$ (blue dashed line), and $p_\alpha = 100\%$ (blue solid line).

an additional term was added of the form $\sigma_{abs} = 0.3326\sqrt{25/E}$, where E is expressed in meV and 0.3326 barn is the absorption cross section of H at 25 meV.

Overall, one can observe a qualitative agreement between the ENDF/B-VII libraries [4,5] for liquid hydrogen at 20 K and the results of the present experiment. It has been recently pointed out [7,38] that the ENDF/B-VII libraries are inaccurate for neutron energies below ca. 10 meV. In particular, in the case of nH we find additional intensity in the experimental data, possibly related to an underestimation in the contribution from translational modes in Ref. [4]. A very good agreement is found for energies between 10 and 200 meV, but above 2 eV. The two rising features in our experimental data around 15–90 meV and 150–350 meV correspond to the $J = 0 \rightarrow 1$ and $J = 0 \rightarrow 3$ recoil-shifted transitions [39,40], respectively, and are found in perfect agreement with previous experimental data [16] and theoretical models [18]. On the contrary, the ENDF/B-VII libraries clearly overestimate the intensity of the higher-energy feature from the $J = 0 \rightarrow 3$ transition. Similarly, the ENDF/B-VII model overestimates the intensity of the hydrogen cross section up to the epithermal region at ca. 2 eV, where both the present experiment and the data in Ref. [16], as well as the Young-Koppel model [41] in the same reference, are relatively featureless. As a consequence of the above discussion, we define the confidence range 10–200 meV where the best agreement is found between experimental data and ENDF/B-VII libraries, to be used in the case of the sample generated within the rig.

A sample of high pH concentration was prepared within the rig and transferred to the VESUVIO cell #2. The experimental cross section obtained from NT is reported in Fig. 6 as blue squares. The quality of experimental data is increased by the use of the sample container #2, with larger sample volume and lower background from the container. The experimental error bars are now compared with two lines, of which the solid line corresponds to pure pH, and the dashed line to $p_\alpha = 96\%$. The experimental data lie within two lines, and the percentage of pH in the sample from the rig is estimated to be $p_\alpha = 98 \pm 2\%$.

3.2. Thermal conductivity measurements on pH and nH

Thermal conductivity measurements on several samples of H_2 from the rig and nH were performed over a period of 7 months. A statistical analysis over the many measurements is representative of the reproducibility of the measurements, as well as the reproducibility of the pH concentration in the sample from the rig. The average values of the wire resistance when the gauge cell was filled with nH and sample from the rig were found to be $R_n = 50.25 \pm 0.10 \Omega$ and $R_r = 45.17 \pm 0.12 \Omega$,

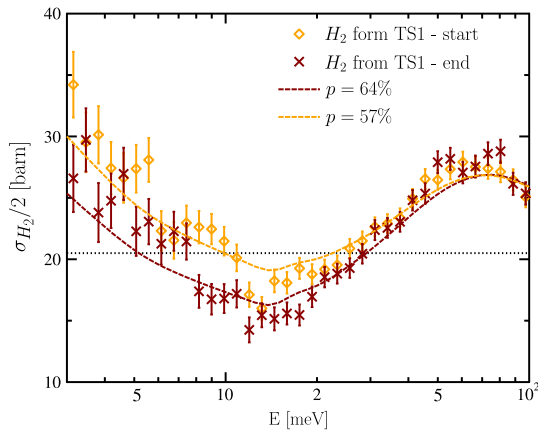


Fig. 7. Neutron cross section per H atom in an unknown mixture of oH and pH obtained from NT. The two spectra correspond to ca. 30-minute-long measurements at the start (dark-red crosses) and at the end (orange diamonds) of the NT experiment on a sample from the TS1 storage bottle. Broken lines correspond to linear combination of oH and pH scattering cross sections obtained from the ENDF/B-VII library. In particular, $p_\alpha = 64\%$ for the dark-red line, and $p = 57\%$ for the orange line.

respectively. These values have been used to define a calibration line to convert the measured resistance of the wire into the concentration of pH in the gas mixture. We assume a linear dependence of the form

$$p_\alpha = f(R_o - R(p_\alpha)), \quad (12)$$

where $R_o = 51.99 \pm 0.14 \Omega$ corresponds to the resistance that the wire would experience if oH was inserted in the gauge cell, and $f = 14.3 \pm 0.4 \Omega^{-1}$. The calibration line expressed by Eq. (12) is based on the general principle expressed by Eq. (6). This approach is based on the knowledge of two reference points, as opposed to Eq. (11) where a single measurement on nH is needed. However, the validity of Eq. (11) is slightly compromised by convection modes in the gauge cell, and the parameter A in Eq. (6) can have a slight dependence upon temperature.

3.3. Additional checks on the validity of the calibration line

The calibration line expressed by Eq. (12) is the result of the following approximations: (i) the resistance of the wire is a linear function of its temperature in the range 77–150 K; and (ii) the thermal conductivity of the mixture is a linear function of the pH concentration. The first approximation is relatively easy to check upon, and we discussed its validity earlier in Section 3.2. The second approximation was discussed in Section 2.3 and in Fig. 5 and we found that its validity is weaker for p_α in the range 50–60%. Similar results were found in previous studies, as in Ref. [42]. It was shown that a full calibration curve of the apparatus can be obtained by letting a gas mixture equilibrate over a long time to three temperatures where p_α is known, e.g., room temperature, liquid nitrogen temperature, and liquid hydrogen temperature. The calibration line found in that work was not linear, with deviations from a linear dependence up to 5%. It was also shown that the sensitivity of the apparatus does not depend on the chosen pressure in the gauge cell, but only on the equilibrium temperature of the wire. The largest differences with respect to a linear calibration are based on the approximate validity of Eq. (10), already shown in Fig. 5. In order to assess the validity of such approximation in our apparatus, we performed additional experiments on an unknown mixture of H_2 , as described below.

A gas mixture from the bottle containing the sample from the TS1 hydrogen moderator was used to evaluate the conversion rate of pH in the buffers of the rig, as discussed in a later section. The resistance of the wire associated with this sample was measured just before a NT experiment, and while removing the gas from the VESUVIO container #2 at the end of the same experiment. The experiment had

Table 1

Concentration of pH in the samples from the ISIS moderators as a function of the time spent in the PTFE-coated storage bottle.

Time [weeks]	TS1		TS2	
	R [Ω]	p_α [%]	R [Ω]	p_α [%]
0	46.05	85 ± 5	45.59	92 ± 5
2	46.52	79 ± 4	45.92	87 ± 5
12	47.74	61 ± 4	46.79	75 ± 4

a duration of about 12 h, and conversion in the gas could be seen in the transmission spectra recorded every ca. 30 min. The resistance measurements before and after the NT experiment, 48.04 Ω and 47.55 Ω respectively, correspond to pH concentrations of $p_\alpha = 57 \pm 4\%$ and $p_\alpha = 64 \pm 4\%$, as the result of the application of Eq. (12). The comparison of the first and last experimental spectra from NT and the corresponding linear combinations of tabulated values from the nuclear libraries is shown in Fig. 7. The quality of the experimental data in this case is compromised by the short measurement. However, good agreement is found between the two sets of data in the region above 10 meV.

3.4. Application to samples from the ISIS moderators

Thermal conductivity measurements performed on samples from TS1 and TS2 hydrogen moderators gave the results reported in Table 1 and Fig. 8(d). The table shows the time evolution of the measured resistance and the corresponding pH concentration as the sample spent time in the storage bottle. The first line of the table corresponds to thermal conductivity measurements performed within a few days from the sample collection. Results show a concentration of pH around 85% and 92% for the samples collected from TS1 and TS2 hydrogen moderators, respectively. Such results should be compared to previous attempts to establish the value of p_α at ISIS, including the analysis of the data from the LOQ [43] incident beam monitor over the last 10 years; the diffraction set-up added to CRISP [44,45] to measure pulse widths over a cycle of experiments; and a comparison between experimental time-of-flight data from OSIRIS [46,47] with corresponding simulations. On the basis of those results, it was assumed that the pH concentration should be around 80–85% in the current TS1 moderator, and that the pH concentration in TS2 hydrogen moderator should be higher. One should remember that the samples characterised in this experiment had been collected from the hydrogen moderators at the end of an experimental cycle, and that the pH concentration can be affected by the history of the cycle. In summary, our measurements agree well with the previous characterisations.

3.5. Conversion of pH in the gas panel

Samples of the gas mixture from the rig were used to test the conversion rate of pH when stored in the components of the gas panel. Conversion rates described below have been modelled by exponential decays of the form

$$R_\alpha(t) = R_r + (R_n - R_r) \left[1 - \exp\left(-\frac{t}{\tau}\right) \right], \quad (13)$$

with τ a characteristic time constant obtained below for every component of the gas panel, and R_n and R_r the resistance measured for nH and sample from the rig, respectively. The constant has been fixed so as to have pH at $t = 0$, and nH for $t \rightarrow \infty$. Collected data are reported in the four panels of Fig. 8, and one should note that the time scales are different in each case.

(a) The main difficulty of the experiment was caused by a high rate of pH conversion while the gas was stored in the buffers of the gas panel. Used buffers were 1-litre SS bottles attached to the rig. Fig. 8(a) shows the conversion rate of pH to oH for two values of the pressure of the gas in the buffers. Experimental data in the case of 508 mbar pressure show a decay constant of $\tau = 9$ min. A strong dependence on the pressure of

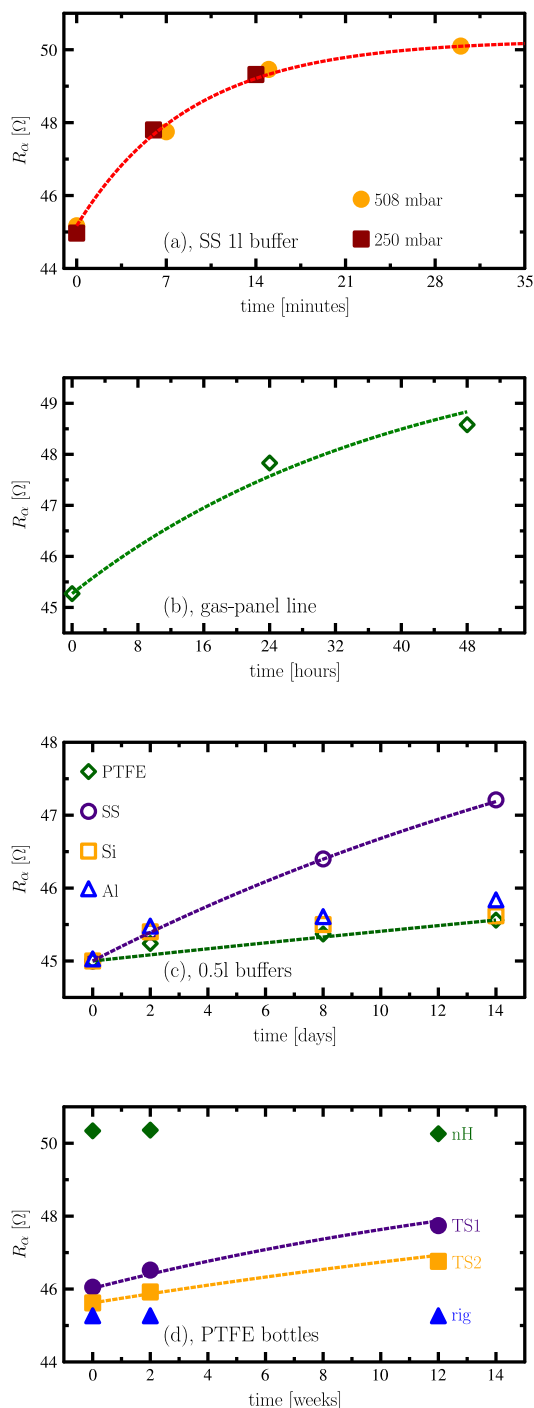


Fig. 8. Conversion rates from pH to oH for several elements of the experimental apparatus. Note the different time scales.

the gas is not observed, as already discussed in Ref. [42]. The buffers of the panel have been extensively used at the start of the experimental campaign, in order to dose the gas sample while loading the VESUVIO container. Each batch of gas spent approximately 10–15 min in the buffer, and a strong suppression of the pH concentration was observed during the following NT experiments.

(b) Samples of gas were monitored while stored in the ca. 3-metre-long gas lines from the generation cell to the VESUVIO container. The gauge cell is approximately 1 metre away from the generation cell along the gas line. Conversion of pH was observed with a decay time $\tau = 40$ h, shown in Fig. 8(b). It is difficult to establish the time a batch of gas spent

in the lines during experimental operations. Our best estimate is that every batch spent less than a minute in the lines while loading. During the NT and thermal conductivity measurements, the largest portion of the gas was stored in the VESUVIO or gauge cells, respectively, and any pH conversion along the lines could be neglected.

(c) After realising that the SS buffers could not be used to dose the gas, we prepared a set of 0.5-litre buffers in different materials or internal coatings to establish which material should be used to minimise pH conversion to oH. In all cases, gas was loaded at a pressure of 250 mbar. Four buffers very similar in volume and shape were considered: SS, SS coated with PTFE, silica, and aluminium. Observed conversion rates are shown in Fig. 8(c). One can see how PTFE coating allows for the lowest conversion rate, with $\tau = 120$ days. The worse case scenario, as expected, corresponded to the SS buffer, where $\tau = 25$ days was found. However, such decay time is much longer than what was found earlier for the 1-litre buffers. This was taken as a proof that the conversion rate strongly depends upon the history of the container, even more than on the thermodynamic variables.

(d) Samples from TS1 and TS2 hydrogen moderators were stored in PTFE-coated bottles, with a volume 1.0 l and at pressure of ca. 7 bar. Fig. 8(d) shows the conversion of the two samples in a period of 12 weeks, compared with measurements performed on the same day of nH and a sample generated from the rig. These results had already been reported in Table 1. It is interesting to note how the conversion rate in this case is higher than what was found for the PTFE-coated buffers in panel (c), possibly suggesting a dependence on the pressure of the gas, now stored at 7–8 bar, as opposed to 250 mbar mentioned in the previous point.

4. Conclusions

We have presented an experimental procedure to establish the concentration of para hydrogen in the hydrogen moderators at ISIS, in both Target Station 1 and Target Station 2. Present results, together with previous characterisations, suggest concentrations of pH greater than or equal to 85% in Target Station 1, and 92% in Target Station 2. These values should be considered lower bounds in our estimation, as we do not have control on a possible conversion of para hydrogen when the samples are collected from the hydrogen moderators. Yet, based on previous estimations, such conversion could be neglected. We estimate our uncertainty to be 5% of the reported values. This procedure was based on neutron transmission experiments aimed at the characterisation of the para-hydrogen concentrations in two reference samples. Such samples were then used as references to convert thermal conductivity measurements in values of para-hydrogen concentration. Moreover, we have discussed an improved procedure where a single reference mixture is needed, say nH, and that could allow *in situ* measurements in the proximity of the moderator, owing to a limited size of the apparatus.

Acknowledgements

This work was partially supported within the CNR-STFC Agreement (2014–2020) concerning collaboration in scientific research at the ISIS pulsed neutron and muon source. We would like to thank Damian Fornalski, Mark Kibble, Chris Goodway, Jon Bones, and Jamie Nutter for their help with setting and running the apparatus. Moreover, we would like to thank Rob Dean, Molly Probert, David Jenkins, and David Haynes for their support in the preparation of the measurements.

References

- [1] <http://www.isis.stfc.ac.uk>, Last accessed on September 2017.
- [2] N. Sullivan, D. Zhou, C. Edwards, Precise and efficient *in situ* ortho — para-hydrogen converter, *Cryogenics* 30 (1990) 734–735.

- [3] F. Fernandez-Alonso, C. Cabrillo, R. Fernández-Perea, F.J. Bermejo, M.A. González, C. Mondelli, E. Farhi, Solid *para*-hydrogen as the paradigmatic quantum crystal: Three observables probed by ultrahigh-resolution neutron spectroscopy, *Phys. Rev. B* 86 (2012) 144524.
- [4] R.E. MacFarlane, New Thermal Neutron Scattering Files for ENDF/B-VI Release 2, Los Alamos National Laboratory Report LA-12639-MS (ENDF-356), 1994.
- [5] M.B. Chadwick, et al., ENDF/B-VII.1 nuclear data for science and technology: Cross sections, covariances, fission product yields and decay data, *Nucl. Data Sheets* 112 (2011) 2887–2996. Special Issue on ENDF/B-VII.1 Library.
- [6] J.A. Young, J.U. Koppel, Slow neutron scattering by molecular hydrogen and deuterium, *Phys. Rev.* 135 (1964) A603–A611.
- [7] K.B. Grammer, et al., Measurement of the scattering cross section of slow neutrons on liquid parahydrogen from neutron transmission, *Phys. Rev. B* 91 (2015) 180301.
- [8] H. Carroll, The interaction of slow neutrons with nuclei, *Phys. Rev.* 60 (1941) 702–709.
- [9] V.F. Sears, Neutron scattering lengths and cross sections, *Neutron News* 3 (1992) 26–37.
- [10] L.-M. Sutherland, J.N. Knudson, M. Mocko, R.M. Renneke, Practical in-situ determination of ortho-para hydrogen ratios via fiber-optic based Raman spectroscopy, *Nucl. Instrum. Methods Phys. Res. A* 810 (2016) 182–185.
- [11] C. Gillis et al., Raman spectroscopy as an ortho-para diagnostic of liquid hydrogen moderators, in: *Talk at the XXII International Collaboration on Advanced Neutron Sources*, 2017.
- [12] M. Hartl, R.C. Gillis, L. Daemen, D.P. Olds, K. Page, S. Carlson, Y. Cheng, T. Hogle, E.B. Iverson, A.J. Ramirez-Cuesta, Y. Lee, G. Muhrer, Hydrogen adsorption on two catalysts for the ortho- to parahydrogen conversion: Cr-doped silica and ferric oxide gel, *Phys. Chem. Chem. Phys.* 18 (2016) 17281–17293.
- [13] W.D. Seiffert, B. Weckermann, R. Misenta, Messung der streuquerschnitte von flüssigem und festem wasserstoff, deuterium und deuteriumhydrid für thermische neutronen, *Z. Naturforsch.* A 25 (1970) 887.
- [14] N. Morishima, D. Mizobuchi, Cross section models for cold neutron scattering from liquid hydrogen and liquid deuterium, *Nucl. Instrum. Methods Phys. Res. A* 350 (1994) 275–285.
- [15] P.A. Egelstaff, P. Schofield, On the evaluation of the thermal neutron scattering law, *Nucl. Sci. Eng.* 12 (1962) 260–270.
- [16] M. Celli, N. Rhodes, A.K. Soper, M. Zoppi, The total neutron cross section of liquid para-hydrogen, *J. Phys.: Condens. Matter* 11 (1999) 10229.
- [17] N. Morishima, A. Nishimura, On the yield of cold and ultracold neutrons for liquid hydrogen at low temperatures near the melting point, *Nucl. Instrum. Methods Phys. Res. A* 426 (1999) 638–641.
- [18] E. Guarini, M. Neumann, U. Bafle, M. Celli, D. Colognesi, E. Farhi, Y. Calzavara, Velocity autocorrelation in liquid parahydrogen by quantum simulations for direct parameter-free computations of neutron cross sections, *Phys. Rev. B* 92 (2015) 104303.
- [19] G. Romanelli, et al., Robust measurement of para-ortho H₂ ratios to characterise the ISIS hydrogen moderators, *J. Phys. Conf. Ser.* (2018), in press.
- [20] <http://www.ckgas.com/>, Last accessed on September 2017.
- [21] B. Evans, J. Bones, C. Goodway, Para-hydrogen Gauge Technical Report, Internal Report, unpublished.
- [22] M.G. Kibble, A.J. Ramirez-Cuesta, C.M. Goodway, B.E. Evans, O. Kirichek, Hydrogen gas sample environment for TOSCA, *J. Phys. Conf. Ser.* 554 (2014) 012006.
- [23] <http://www.sigmaaldrich.com/catalog/product/supelco/20631>, Last accessed on September 2017.
- [24] <http://www.isis.stfc.ac.uk/Pages/VESUVIO.aspx>, Last accessed on September 2017.
- [25] G. Romanelli, M. Krzystyniak, R. Senesi, D. Raspino, J. Boxall, D. Pooley, S. Moorby, E. Schooneveld, N.J. Rhodes, C. Andreani, F. Fernandez-Alonso, Characterisation of the incident beam and current diffraction capabilities on the VESUVIO spectrometer, *Meas. Sci. Technol.* 28 (2017) 095501.
- [26] C. Andreani, M. Krzystyniak, G. Romanelli, R. Senesi, F. Fernandez-Alonso, Electron-volt neutron spectroscopy: beyond fundamental systems, *Adv. Phys.* 66 (2017) 1–73.
- [27] A. Parmentier, J.J. Shephard, G. Romanelli, R. Senesi, C.G. Salzmann, C. Andreani, Evolution of hydrogen dynamics in amorphous ice with density, *J. Phys. Chem. Lett.* 6 (2015) 2038–2042. PMID: 26266499.
- [28] A.I. Kolesnikov, G.F. Reiter, N. Choudhury, T.R. Prisk, E. Mamontov, A. Podlesnyak, G. Ehlers, A.G. Seel, D.J. Wesolowski, L.M. Anovitz, Quantum tunneling of water in beryl: A new state of the water molecule, *Phys. Rev. Lett.* 116 (2016) 167802.
- [29] M. Krzystyniak, K. Druzicki, G. Romanelli, M.J. Gutmann, S. Rudic, S. Imberti, F. Fernandez-Alonso, Nuclear dynamics and phase polymorphism in solid formic acid, *Phys. Chem. Chem. Phys.* 19 (2017) 9064–9074.
- [30] C. Andreani, G. Romanelli, R. Senesi, Direct measurements of quantum kinetic energy tensor in stable and metastable water near the triple point: An experimental benchmark, *J. Phys. Chem. Lett.* 7 (2016) 2216–2220.
- [31] L.A. Rodríguez Palomino, J. Dawidowski, J.I. Márquez Damián, G.J. Cuello, G. Romanelli, M. Krzystyniak, Neutron total cross-section of hydrogenous and deuterated 1- and 2-propanol and n-butanol measured using the vesuvio spectrometer, *Nucl. Instrum. Methods Phys. Res. A* 870 (2017) 84–89.
- [32] H.W. Woolley, R.B. Scott, F. Brickwedde, *Compilation of Thermal Properties of Hydrogen in its Various Isotopic and Ortho-para Modifications*, National Bureau of Standards, 1948.
- [33] R. McCarty, J. Hord, H. Roder, *Selected Properties of Hydrogen (Engineering Design Data)*, Final report, 1981.
- [34] A. Eucken, Über die temperaturabhängigkeit der wärmeleitfähigkeit fester nichtmetalle, *Ann. Phys.* 339 (1911) 185–221.
- [35] <http://www.lakeshore.com/Documents/F03800-00.pdf>, Last accessed on September 2017.
- [36] N. Todreas, M. Kazimi, *Nuclear Systems Volume I: Thermal Hydraulic Fundamentals*, vol. 1, second ed., CRC Press, 2011.
- [37] E. Udoetok, Thermal conductivity of binary mixtures of gases, *Front. Heat Mass Transfer* 4 (2013).
- [38] R. Granada et al., New neutron scattering kernels for liquid hydrogen and deuterium, in: *Talk at the XXII International Collaboration on Advanced Neutron Sources*, 2017.
- [39] W. Langel, D.L. Price, R.O. Simmons, P.E. Sokol, Inelastic neutron scattering from liquid and solid hydrogen at high momentum transfer, *Phys. Rev. B* 38 (1988) 11275–11283.
- [40] W.L. Whittemore, A.W. McReynolds, Effects of chemical binding on the neutron cross section of hydrogen, *Phys. Rev.* 113 (1959) 806–808.
- [41] J.A. Young, J.U. Koppel, Slow neutron scattering by molecular hydrogen and deuterium, *Phys. Rev.* 135 (1964) A603–A611.
- [42] A.T. Stewart, G.L. Squires, Analysis of ortho- and para-hydrogen mixtures by the thermal conductivity method, *J. Sci. Instrum.* 32 (1955) 26.
- [43] G. Škoro, Cold Moderators at ISIS, Vienna, Austria, 2016.
- [44] <http://www.isis.stfc.ac.uk/Pages/CRISP.aspx>, Last accessed on September 2017.
- [45] R. Bewley et al., 2016 TS-1 baseline: experiment vs. simulatons, Talk at 3rd ISIS TRAMSNEG Meeting.
- [46] <http://www.isis.stfc.ac.uk/Pages/OSIRIS.aspx>, Last accessed on September 2017.
- [47] R. Bewley et al., 2016 TS-1 baseline: experiment vs. simulatons, Talk at 2nd ISIS TRAMSNEG Meeting.